

Cite this: *Catal. Sci. Technol.*, 2014,
4, 224

Competition of selective catalytic reduction and non selective catalytic reduction over $\text{MnO}_x/\text{TiO}_2$ for NO removal: the relationship between gaseous NO concentration and N_2O selectivity†

Shijian Yang,^{ab} Yuwu Fu,^a Yong Liao,^a Shangchao Xiong,^a Zan Qu,^c Naiqiang Yan^c
and Junhua Li^{*b}

In this work, a novel phenomenon was discovered that N_2O selectivity of NO reduction over $\text{MnO}_x/\text{TiO}_2$ was related to the concentration of gaseous NO and that lower concentration of gaseous NO would cause higher N_2O selectivity. *In situ* DRIFTS and transient reaction studies demonstrated that both the Eley–Rideal mechanism (the reaction of over-activated NH_3 with gaseous NO) and the Langmuir–Hinshelwood mechanism (the reaction of adsorbed NO_3^- with adsorbed NH_3 on the adjacent sites) could contribute to the formation of N_2O . Kinetic study demonstrated that N_2O selectivity would be independent of gaseous NO concentration if NO reduction over $\text{MnO}_x/\text{TiO}_2$ mainly followed the Langmuir–Hinshelwood mechanism. If NO reduction over $\text{MnO}_x/\text{TiO}_2$ mainly followed the Eley–Rideal mechanism, there was competition between the selective catalytic reduction (SCR) reaction and non selective catalytic reduction (NSCR) reaction. As gaseous NO concentration increased, more $-\text{NH}_2$ was used to reduce gaseous NO to form N_2 and the further oxidization of $-\text{NH}_2$ to $-\text{NH}$ was restrained, resulting in an obvious decrease of N_2O selectivity. The Eley–Rideal mechanism played an important role in NO reduction over $\text{MnO}_x/\text{TiO}_2$, especially at higher temperatures. Therefore, N_2O selectivity of the low temperature SCR reaction over $\text{MnO}_x/\text{TiO}_2$ decreased especially at higher temperatures after the increase of gaseous NO concentration.

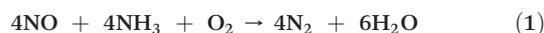
Received 30th August 2013,
Accepted 8th October 2013

DOI: 10.1039/c3cy00648d

www.rsc.org/catalysis

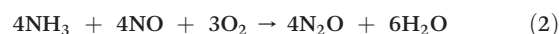
1. Introduction

Nitrogen oxides (NO and NO_2), emitted from automobiles and stationary sources, greatly contribute to the formation of smog, acid rain and ozone.¹ Selective catalytic reduction (SCR) of NO with NH_3 has been an efficient technique for the control of NO_x emission from coal fired power plants and automobiles.² The standard SCR process is based on the following reaction between NH_3 and NO:³



$\text{V}_2\text{O}_5\text{-WO}_3(\text{MoO}_3)/\text{TiO}_2$ has been widely used as a SCR catalyst to control the emission of NO from stationary coal

fired power plants for several decades.² The temperature window of $\text{V}_2\text{O}_5\text{-WO}_3(\text{MoO}_3)/\text{TiO}_2$ is about 300–400 °C, so the SCR unit is located upstream of the desulfurizer and electrostatic precipitator in order to avoid reheating of the flue gas.⁴ However, retrofitting the SCR devices into existing systems is difficult because the space and access in many power plants are extremely limited.⁵ Therefore, there has been strong demand in developing highly active SCR catalysts at low temperatures, which will be placed downstream of the electrostatic precipitator and desulfurizer.⁶ Mn based catalysts, for example $\text{MnO}_x\text{-CeO}_2$,^{7,8} $\text{MnO}_2/\text{TiO}_2$,^{9–13} $\text{MnO}_x\text{-CeO}_2/\text{TiO}_2$ ¹⁴ and $\text{Fe}_2\text{O}_3\text{-MnO}_2/\text{TiO}_2$,¹⁵ show excellent low temperature SCR activity among the first row transition metal based catalysts.^{16–20} However, some N_2O would form during the low temperature SCR reaction over Mn based catalysts.^{6,7,21} The non selective catalytic reduction (NSCR) reaction is based on the following reaction between NH_3 and NO:²²



N_2O is now considered as a pollutant due to its greenhouse effect and its depletion of the ozone layer.^{22–25} However, only a little work focused on the mechanism of N_2O formation during the low temperature SCR over Mn based

^a School of Environmental and Biological Engineering, Nanjing University of Science and Technology, Nanjing, 210094, PR China.

E-mail: yangshijiangsq@163.com

^b State Key Joint Laboratory of Environment Simulation and Pollution Control (SKLESPC), School of Environment, Tsinghua University, Beijing, 100084, PR China. E-mail: lijunhua@tsinghua.edu.cn; Fax: +86 10 62771093;

Tel: +86 10 62771093

^c School of Environmental Science and Engineering, Shanghai Jiao Tong University, Shanghai, 200240, PR China

† Electronic supplementary information (ESI) available. See DOI: 10.1039/c3cy00648d

catalyst.²¹ Some groups have demonstrated that one of the two N atoms in N₂O originates from NH₃ and the other from NO under the SCR conditions.^{3,22} However, there is no agreement on the mechanism of N₂O formation: by (1) reaction of gaseous NO with over-activated NH₃ (-NH) to N₂O (*i.e.* the Eley-Rideal mechanism), or (2) adsorption of NO₃⁻ on the adjacent sites of adsorbed NH₃, followed by reaction to an activated transition state (*i.e.* NH₄NO₃) and then decomposition to N₂O (*i.e.* the Langmuir-Hinshelwood mechanism).³ Recently, a novel phenomenon has been found that N₂O selectivity of the low temperature SCR reaction over MnO_x/TiO₂ was related to the concentration of gaseous NO. N₂O selectivity obviously decreased after the increase of gaseous NO concentration in the inlet. Herein, the mechanism of N₂O formation during the low temperature SCR reaction over MnO_x/TiO₂ was studied, and the effect of NO concentration on N₂O selectivity was investigated.

2. Experimental

2.1 Catalyst preparation

MnO_x/TiO₂ (Mn loading was 5 wt%) was prepared by the impregnation method using Degussa TiO₂ P25 as support and manganese nitrate as precursor. The sample was dried at 110 °C for 12 h, and it was then calcined at 500 °C under air atmosphere for 3 h.

2.2 Catalytic test

The reduction of NO was performed on a fixed-bed quartz tube reactor (6 mm of internal diameter). The catalyst with 40–60 mesh was placed on the quartz wool held in the reactor, which was heated by a vertical electrical furnace. The total flow rate was 200 mL min⁻¹ (room temperature), and the mass of catalyst was 200 mg. The corresponding gas hourly space velocity (GHSV) was 6 × 10⁴ cm³ g⁻¹ h⁻¹ (*i.e.* 75 000 h⁻¹). The feed contained 500 or 1000 ppm of NO, 500 or 1000 ppm of NH₃, 2% of O₂, and balance of N₂. The concentrations of NO, NO₂, NH₃ and N₂O in the outlet were continually monitored by an FTIR spectrometer (MKS Instruments). The ratios of NO_x and NH₃ conversion, the amount of N₂ formed and N₂O selectivity were calculated using the following equations:

$$\text{NO}_x \text{ conversion} = \frac{[\text{NO}_x]_{\text{in}} - [\text{NO}_x]_{\text{out}}}{[\text{NO}_x]_{\text{in}}} \quad (3)$$

$$\text{NH}_3 \text{ conversion} = \frac{[\text{NH}_3]_{\text{in}} - [\text{NH}_3]_{\text{out}}}{[\text{NH}_3]_{\text{in}}} \quad (4)$$

$$\text{N}_2 \text{ formation} = \frac{[\text{NH}_3]_{\text{in}} - [\text{NH}_3]_{\text{out}} + [\text{NO}_x]_{\text{in}} - [\text{NO}_x]_{\text{out}} - 2[\text{N}_2\text{O}]_{\text{out}}}{2} \quad (5)$$

$$\text{N}_2\text{O selectivity} = \frac{2[\text{N}_2\text{O}]_{\text{out}}}{[\text{NH}_3]_{\text{in}} + [\text{NO}_x]_{\text{in}} - [\text{NH}_3]_{\text{out}} - [\text{NO}_x]_{\text{out}}} \quad (6)$$

where, [NH₃]_{in} and [NO_x]_{in} were the concentrations of NH₃ and NO_x (including NO and NO₂) in the inlet, and [NH₃]_{out}, [NO_x]_{out} and [N₂O]_{out} were the concentrations of NH₃, NO_x (including NO and NO₂) and N₂O in the outlet.

2.3 In situ DRIFTS study

In situ DRIFT spectra were recorded on a Fourier transform infrared spectrometer (FTIR, Nicolet NEXUS 870) equipped with a smart collector and an MCT detector cooled by liquid N₂.²⁶ The catalyst was finely ground and placed in a ceramic crucible and manually pressed. The FTIR spectra were recorded by accumulating 100 scans with a resolution of 4 cm⁻¹.

3. Results

3.1 SCR performance of MnO_x/TiO₂ for the low temperature SCR reaction

The performance of MnO_x/TiO₂ for the low temperature SCR reaction at 100–250 °C is shown in Fig. 1. Both the ratio of NO conversion and N₂O selectivity increased with the increase of reaction temperature, which is consistent with previous research on the low temperature SCR reaction over

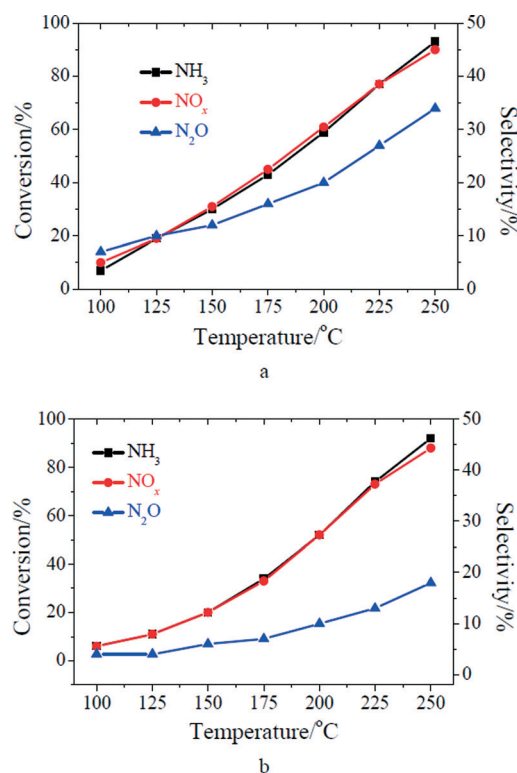


Fig. 1 SCR performance of MnO_x/TiO₂: (a) [NO] = [NH₃] = 500 ppm; (b) [NO] = [NH₃] = 1000 ppm. Reaction conditions: [O₂] = 2%, catalyst mass = 200 mg, total flow rate = 200 mL min⁻¹, GHSV = 60 000 cm³ g⁻¹ h⁻¹.

$\text{MnO}_x/\text{TiO}_2$.^{13,27,28} As the concentrations of NO and NH_3 in the inlet increased from 500 to 1000 ppm, the ratios of NO and NH_3 conversion over $\text{MnO}_x/\text{TiO}_2$ slightly decreased. A similar result once happened on Mn-Fe spinel.⁶ However, N_2O selectivity obviously decreased after the increase of the concentrations of gaseous NO and NH_3 especially at higher temperatures (shown in Fig. 1). It suggests that N_2O selectivity of the low temperature SCR reaction over $\text{MnO}_x/\text{TiO}_2$ was related to the concentrations of gaseous NO and NH_3 in the inlet. This phenomenon was seldom previously reported in the literature.

3.2 Effect of gaseous NO concentration on N_2O selectivity

Fig. 2 shows the effect of gaseous NO concentration on NH_3 conversion and N_2O formation. As shown in Fig. 2a, little NH_3 can be oxidized over $\text{MnO}_x/\text{TiO}_2$ below 175 °C in the absence of NO. With the increase of reaction temperature from 175 to 250 °C, NH_3 oxidation was promoted (shown in Fig. 2a). However, more than 50% of NH_3 was oxidized to N_2O at 200–250 °C (shown in Fig. 2b).

As 500 ppm of NO was introduced, NH_3 conversion over $\text{MnO}_x/\text{TiO}_2$ was promoted (shown in Fig. 2a). Meanwhile, N_2O selectivity of $\text{MnO}_x/\text{TiO}_2$ for the SCR reaction was much less than that for NH_3 oxidation at 200–250 °C. As the concentration of gaseous NO increased from 500 to 1000 ppm, NH_3 conversion was further promoted (shown in Fig. 2a).

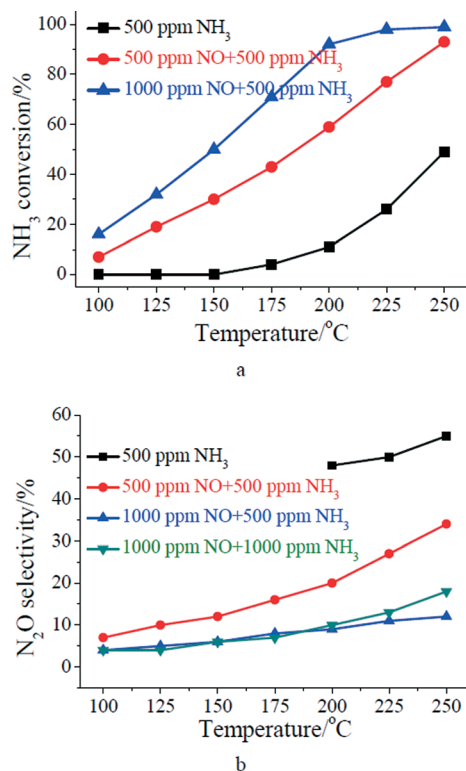


Fig. 2 Effect of NO concentration on: (a) NH_3 conversion; (b) N_2O selectivity. Reaction conditions: $[\text{O}_2] = 2\%$, catalyst mass = 200 mg, total flow rate = 200 mL min^{-1} , GHSV = 60 000 $\text{cm}^3 \text{g}^{-1} \text{h}^{-1}$.

Meanwhile, the formation of N_2O over $\text{MnO}_x/\text{TiO}_2$ was further restrained (shown in Fig. 2b). It suggests that N_2O selectivity over $\text{MnO}_x/\text{TiO}_2$ was related to the concentration of gaseous NO.

3.3 In situ DRIFTS study

3.3.1 Transient reaction at 150 °C. $\text{MnO}_x/\text{TiO}_2$ was first treated with 500 ppm of NH_3 at 150 °C for 30 min followed by N_2 purged for 5 min. 500 ppm of NO and 2% of O_2 were then introduced into the IR cell (shown in Fig. 3a). After the adsorption of NH_3 , five characteristic vibrations at 1680, 1600, 1437, 1206 and 1165 cm^{-1} appeared on $\text{MnO}_x/\text{TiO}_2$. The bands at 1600 and 1206 cm^{-1} were assigned to coordinated NH_3 bound to the Lewis acid sites, and the bands at 1680

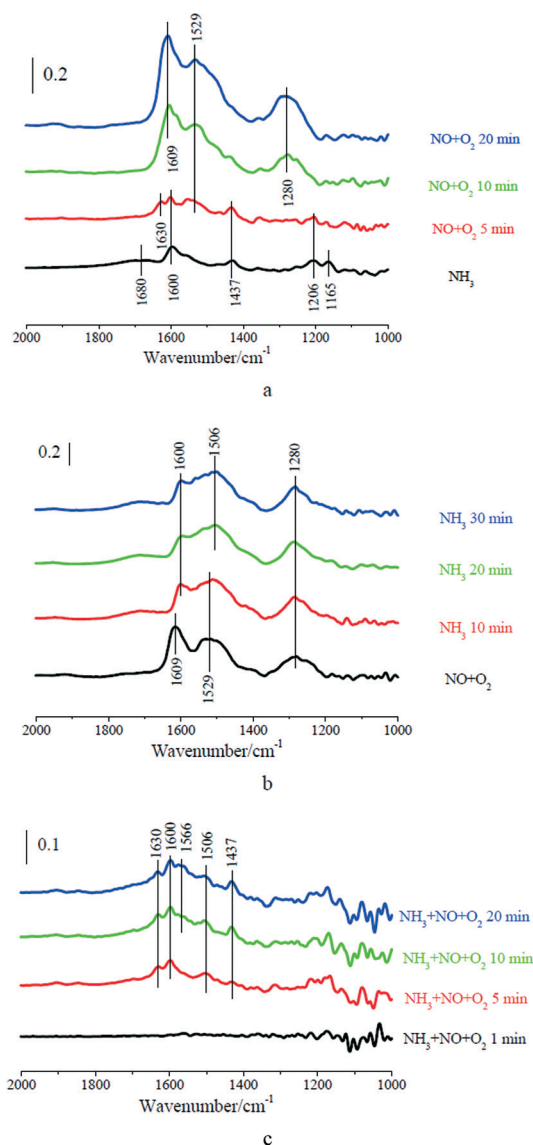


Fig. 3 (a) DRIFT spectra taken at 150 °C upon passing NO + O_2 over NH_3 presorbed $\text{MnO}_2/\text{TiO}_2$; (b) DRIFT spectra taken at 150 °C upon passing NH_3 over NO + O_2 presorbed $\text{MnO}_2/\text{TiO}_2$; (c) DRIFT spectra taken at 150 °C upon passing NH_3 + NO + O_2 over $\text{MnO}_2/\text{TiO}_2$.

and 1437 cm^{-1} were attributed to ionic NH_4^+ bound to the Brønsted acid sites.^{8,10} The band at 1165 cm^{-1} could be attributed to $-\text{NH}_2$, which resulted from the activation of coordinated NH_3 bound to the Lewis acid sites.²⁹ After $\text{NO} + \text{O}_2$ passed over NH_3 pretreated $\text{MnO}_x/\text{TiO}_2$, the bands at 1680 , 1600 , 1437 , 1206 and 1165 cm^{-1} corresponding to adsorbed ammonia species gradually diminished. Meanwhile, three characteristic vibrations at 1609 , 1529 and 1280 cm^{-1} appeared. The band at 1609 cm^{-1} was assigned to monodentate nitrite, and the bands at 1529 and 1280 cm^{-1} were attributed to bidentate nitrate.³⁰ Moreover, adsorbed H_2O , which is the product of the SCR reaction, appeared at 1630 cm^{-1} . These bands suggest that adsorbed NH_3 can react with gaseous NO (*i.e.* the Eley–Rideal mechanism). The concentrations of N_2O and NO in the outlet during the transient reaction were simultaneously recorded (shown in Fig. 4a). After $\text{NO} + \text{O}_2$ passed over NH_3 pretreated $\text{MnO}_x/\text{TiO}_2$, NO concentration gradually increased to about 480 ppm . Meanwhile, the concentration of N_2O in the outlet rapidly increased to about 30 ppm , and it then gradually decreased to the background of N_2O in NO (9 ppm) (shown in Fig. 4a). It suggests that the reaction between adsorbed NH_3 and gaseous NO (*i.e.* the Eley–Rideal mechanism) at $150\text{ }^\circ\text{C}$ can produce N_2O .

Then, the reactants were introduced to $\text{MnO}_x/\text{TiO}_2$ in the reverse order. $\text{MnO}_x/\text{TiO}_2$ was first treated with 500 ppm of NO and 2% of O_2 for 30 min at $150\text{ }^\circ\text{C}$ followed by N_2 purged for 5 min . 500 ppm of NH_3 was then introduced into the IR cell (shown in Fig. 3b). After the adsorption of $\text{NO} + \text{O}_2$ at $150\text{ }^\circ\text{C}$, $\text{MnO}_x/\text{TiO}_2$ was mainly covered by monodentate

nitrite (1609 cm^{-1}) and bidentate nitrate (1529 and 1280 cm^{-1}). After NH_3 was introduced into the cell, the bands corresponding to monodentate nitrite (at 1609 cm^{-1}) and bidentate nitrate (1529 cm^{-1}) firstly shifted to 1600 and 1506 cm^{-1} . Then, the intensities of the two bands gradually decreased (shown in Fig. 3b). They suggest that adsorbed NO_x can react with adsorbed NH_3 (*i.e.* the Langmuir–Hinshelwood mechanism). The concentrations of N_2O and NH_3 in the outlet during the transient reaction were simultaneously recorded (shown in Fig. 4b). After NH_3 was introduced to $\text{NO} + \text{O}_2$ pretreated $\text{MnO}_x/\text{TiO}_2$ for 5 min , little NH_3 was observed. Meanwhile, the concentration of N_2O in the outlet rapidly increased to about 13 ppm after the introduction of NH_3 , and it then gradually decreased to about 5 ppm in 60 min . It suggests that the reaction between adsorbed NH_3 and adsorbed NO_x (*i.e.* the Langmuir–Hinshelwood mechanism) can also produce N_2O . Fig. 3b shows that the decrease of the band at 1600 cm^{-1} corresponding to adsorbed NH_4NO_2 was much faster than that at 1506 cm^{-1} corresponding to adsorbed NH_4NO_3 . It suggests that the reaction through the nitrite route was faster than that through the nitrate route, which was consistent with the result of Mn–Fe spinel.⁶ Previous research demonstrated that the product of the nitrite route was N_2 , while that of nitrate route was N_2O .²²

Finally, the IR spectra during the SCR reaction (*i.e.* 500 ppm of NH_3 , 500 ppm of NO and 2% of O_2 were simultaneously introduced) at $150\text{ }^\circ\text{C}$ were recorded. As shown in Fig. 3c, adsorbed H_2O (at 1630 cm^{-1}), coordinated NH_3 or adsorbed NH_4NO_2 (at 1600 cm^{-1}), adsorbed NH_4NO_3 (at 1566 and 1506 cm^{-1}) and ionic NH_4^+ (at 1437 cm^{-1}) were all observed. It suggests that both the Langmuir–Hinshelwood mechanism and the Eley–Rideal mechanism could happen at $150\text{ }^\circ\text{C}$.

3.3.2 Transient reaction at $250\text{ }^\circ\text{C}$. $\text{MnO}_x/\text{TiO}_2$ was first treated with 500 ppm of NH_3 for 30 min at $250\text{ }^\circ\text{C}$, and 500 ppm of NO and 2% of O_2 were then introduced into the IR cell (shown in Fig. 5a). After the adsorption of NH_3 , $\text{MnO}_x/\text{TiO}_2$ was mainly covered by coordinated NH_3 bound to the Lewis acid sites (at 1602 cm^{-1}). After $\text{NO} + \text{O}_2$ passed over NH_3 pretreated $\text{MnO}_x/\text{TiO}_2$, coordinated NH_3 rapidly diminished, and adsorbed H_2O (at 1620 cm^{-1}) appeared. Then, $\text{MnO}_x/\text{TiO}_2$ was mainly covered by monodentate nitrite (at 1607 cm^{-1}) and monodentate nitrate (1559 cm^{-1}).³⁰ The concentrations of NH_3 , N_2O , NO and NO_2 during the transient reaction were simultaneously recorded (shown in Fig. 6a). As NH_3 was introduced to $\text{MnO}_x/\text{TiO}_2$, about 90 ppm of N_2O was observed, which resulted from the oxidation of NH_3 by the lattice oxygen of $\text{MnO}_x/\text{TiO}_2$. After $\text{NO} + \text{O}_2$ passed over NH_3 pretreated $\text{MnO}_x/\text{TiO}_2$ at $250\text{ }^\circ\text{C}$, N_2O concentration rapidly increased from 90 to 160 ppm , and it then decreased to the background of N_2O in NO (9 ppm). The concentration of N_2O from the transient reaction at $250\text{ }^\circ\text{C}$ was much higher than that at $150\text{ }^\circ\text{C}$. It suggests that the formation of N_2O from the Eley–Rideal mechanism was obviously promoted with the increase of reaction temperature.

Then, the reactants were introduced to $\text{MnO}_x/\text{TiO}_2$ in the reverse order. $\text{MnO}_x/\text{TiO}_2$ was first treated with 500 ppm of

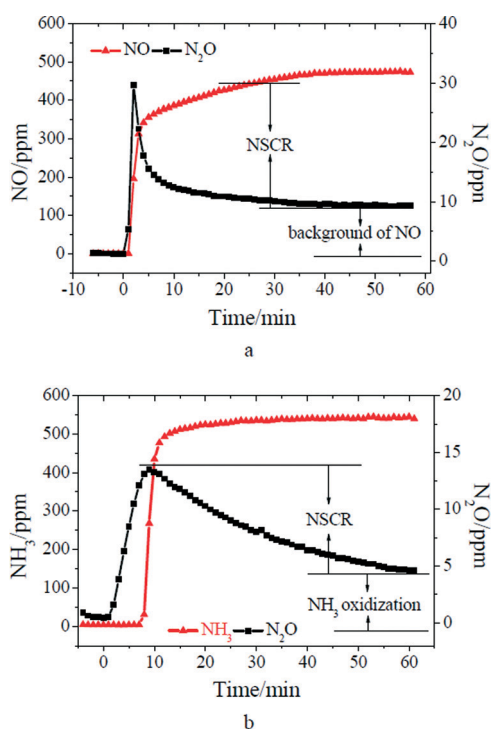


Fig. 4 (a) Transient reaction taken at $150\text{ }^\circ\text{C}$ upon passing $\text{NO} + \text{O}_2$ over NH_3 presorbed $\text{MnO}_2/\text{TiO}_2$; (b) Transient reaction taken at $150\text{ }^\circ\text{C}$ upon passing NH_3 over $\text{NO} + \text{O}_2$ presorbed $\text{MnO}_2/\text{TiO}_2$.

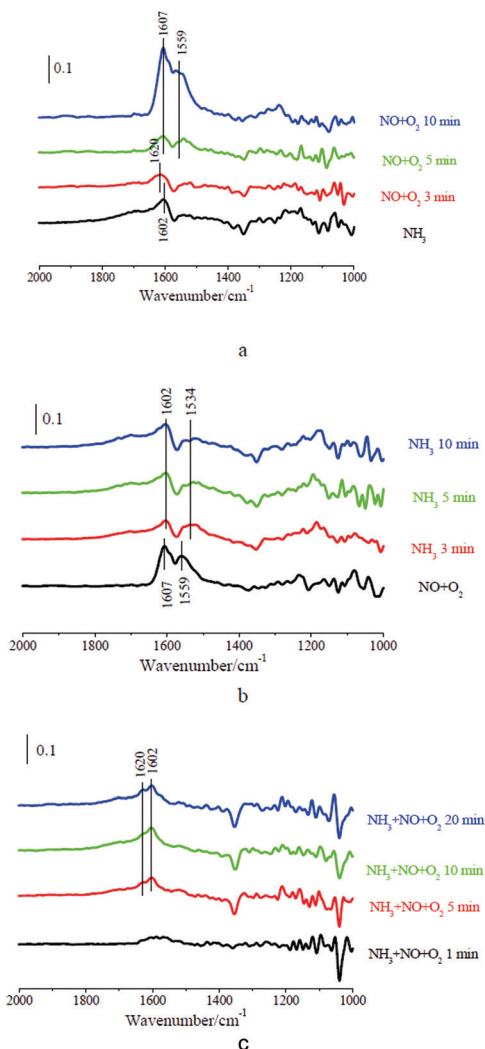


Fig. 5 (a) DRIFT spectra taken at 250 °C upon passing NO + O₂ over NH₃ presorbed MnO_x/TiO₂; (b) DRIFT spectra taken at 250 °C upon passing NH₃ over NO + O₂ presorbed MnO_x/TiO₂; (c) DRIFT spectra taken at 250 °C upon passing NH₃ + NO + O₂ over MnO_x/TiO₂.

NO and 2% of O₂ for 30 min followed by N₂ purged for 5 min at 250 °C. 500 ppm of NH₃ was then introduced into the IR cell (shown in Fig. 5b). After the adsorption of NO + O₂ at 250 °C, MnO_x/TiO₂ was mainly covered by monodentate nitrite (1607 cm⁻¹) and monodentate nitrate (1559 cm⁻¹). After NH₃ was introduced into the cell, the band at 1607 cm⁻¹ corresponding to monodentate nitrite (at 1607 cm⁻¹) rapidly diminished. However, monodentate nitrate (1559 cm⁻¹) firstly shifted to 1534 cm⁻¹. Then, it gradually diminished. Finally, MnO_x/TiO₂ was mainly covered by coordinated NH₃ (at 1602 cm⁻¹). The concentrations of N₂O and NH₃ during the transient reaction were simultaneously recorded (shown in Fig. 6b). After NH₃ was introduced to NO + O₂ pretreated MnO_x/TiO₂ for 10 min, NH₃ in the outlet was observed. Meanwhile, the concentration of N₂O in the outlet rapidly increased to about 110 ppm after the introduction of NH₃, and it then gradually decreased to about 90 ppm in 50 min (shown in Fig. 6b). In this case, the origination of N₂O from

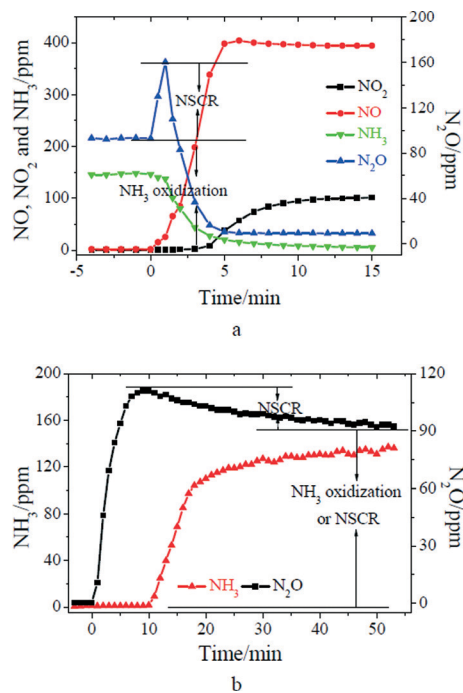


Fig. 6 (a) Transient reaction taken at 250 °C upon passing NO + O₂ over NH₃ presorbed MnO_x/TiO₂; (b) Transient reaction taken at 250 °C upon passing NH₃ over NO + O₂ presorbed MnO_x/TiO₂.

NH₃ oxidation or the Langmuir–Hinshelwood mechanism was difficult to be differentiated. However, the concentration of N₂O in the first 5 min was slightly higher than the concentration of N₂O from the oxidation of 500 ppm of NH₃. It suggests that the Langmuir–Hinshelwood mechanism can also contribute to N₂O formation at 250 °C.

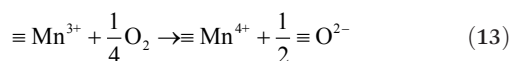
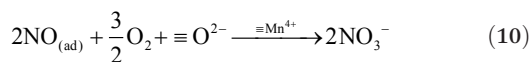
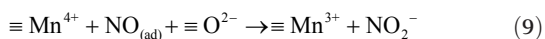
Finally, the IR spectra during the SCR reaction (*i.e.* 500 ppm of NH₃, 500 ppm of NO and 2% of O₂ were simultaneously introduced) at 250 °C were recorded. As shown in Fig. 5c, only adsorbed H₂O (at 1620 cm⁻¹) and coordinated NH₃ or adsorbed NH₄NO₂ (at 1602 cm⁻¹) can be clearly detected. However, the band at 1534 cm⁻¹ corresponding to adsorbed NH₄NO₃ can not be observed. Fig. 5a shows that the disappearance of NH₄NO₃ was much slower than that of NH₄NO₂. It suggests that NH₄NO₃ did not form during NO reduction over MnO_x/TiO₂ at 250 °C. Therefore, the contribution of NH₄NO₃ decomposition to N₂O formation can be neglected and N₂O formation at 250 °C mainly resulted from the Eley–Rideal mechanism.

4. Discussion

4.1 Mechanism of N₂O formation

4.1.1 N₂O formation from the Langmuir–Hinshelwood mechanism. The reduction of NO (including the SCR reaction and the NSCR reaction) through the Langmuir–Hinshelwood mechanism can be approximately described as:^{3,6,22}





Reaction 7 is the adsorption of gaseous ammonia on the acid sites (*i.e.* Brønsted acid sites and Lewis acid sites) to form adsorbed ammonia species including ionic NH_4^+ and coordinated NH_3 . Reaction 8 is the physical adsorption of gaseous NO on $\text{MnO}_x/\text{TiO}_2$. Then, adsorbed NO is oxidized by Mn^{4+} on $\text{MnO}_x/\text{TiO}_2$ to form adsorbed NO_2^- (*i.e.* reaction 9). Reaction 10 is the oxidation of adsorbed NO by Mn^{4+} on $\text{MnO}_x/\text{TiO}_2$ to NO_3^- . Subsequently, adsorbed NO_2^- and NO_3^- react with adsorbed NH_3 species on the adjacent sites to form NH_4NO_2 and NH_4NO_3 (*i.e.* reactions 11 and 12), respectively. Finally, NH_4NO_2 and NH_4NO_3 are decomposed to N_2 and N_2O , respectively. Reaction 13 is the regeneration of Mn^{4+} on $\text{MnO}_x/\text{TiO}_2$.

The kinetic equations of the formation of N_2 and N_2O over $\text{MnO}_x/\text{TiO}_2$ through the Langmuir–Hinshelwood mechanism can be approximately described as:

$$\frac{d[\text{N}_2]}{dt} = -\frac{d[\text{NH}_4\text{NO}_2]}{dt} = k_1[\text{NH}_4\text{NO}_2] \quad (14)$$

$$\frac{d[\text{N}_2\text{O}]}{dt} = -\frac{d[\text{NH}_4\text{NO}_3]}{dt} = k_2[\text{NH}_4\text{NO}_3] \quad (15)$$

where, k_1 , k_2 , $[\text{NH}_4\text{NO}_2]$ and $[\text{NH}_4\text{NO}_3]$ are the decomposition rate constants of NH_4NO_2 and NH_4NO_3 , and the concentrations of NH_4NO_2 and NH_4NO_3 on $\text{MnO}_x/\text{TiO}_2$, respectively.

$[\text{NH}_4\text{NO}_2]$ and $[\text{NH}_4\text{NO}_3]$ are mainly related to the concentrations of NO adsorbed ($[\text{NO}_{(\text{ad})}]$) and Mn^{4+} on $\text{MnO}_x/\text{TiO}_2$ (the deduction is shown in the ESI†). The GHSV used in this work was quite high and there were generally large amounts of NO_x and NH_3 in the outlet (shown in Fig. 7a and b), so $\text{MnO}_x/\text{TiO}_2$ was almost saturated with the adsorption of NO and NH_3 . Furthermore, there is generally agreement that the SCR reaction starts with the adsorption of NH_3 , which is very strong compared to the adsorption of

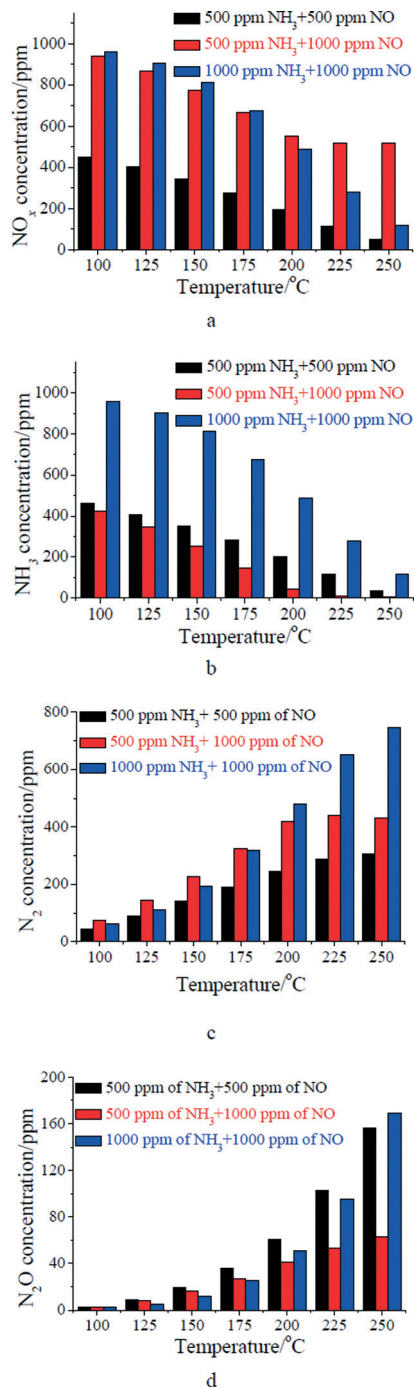
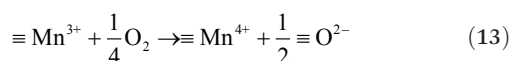
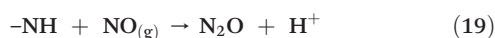
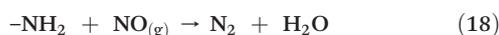
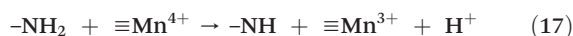
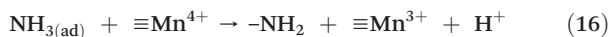


Fig. 7 Concentrations of NO_x (a), NH_3 (b), N_2 formed (c) and N_2O (d) in the outlet of the reactor. Reaction conditions: $[\text{O}_2] = 2\%$, catalyst mass = 200 mg, total flow rate = 200 mL min^{-1} , GHSV = 60 000 $\text{cm}^3 \text{g}^{-1} \text{h}^{-1}$.

$\text{NO} + \text{O}_2$ and the products.³ Thus, the increase of gaseous NO concentration from 500 to 1000 ppm could not break the adsorption equilibrium of NH_3 and NO. It suggests that $[\text{NO}_{(\text{ad})}]$ and $[\text{NH}_{3(\text{ad})}]$ would not vary after increasing the concentrations of gaseous NO and NH_3 . As a result, the concentrations of NH_4NO_2 and NH_4NO_3 on $\text{MnO}_x/\text{TiO}_2$ were independent of the concentrations of gaseous NO and NH_3 .

4.1.2 N₂O formation from the Eley–Rideal mechanism.

The reduction of NO (including the SCR reaction and the NSCR reaction) through the Eley–Rideal mechanism can be approximately described as:^{3,6,22}



Reaction 16 is the activation of adsorbed ammonia species by Mn⁴⁺ on MnO_x/TiO₂ to form amide species (-NH₂). -NH₂ on MnO_x/TiO₂ can be further oxidized to -NH (*i.e.* reaction 17). Then, gaseous NO was reduced by -NH₂ and -NH on the surface to form N₂ and N₂O (*i.e.* reactions 18 and 19), respectively.

The kinetic equation of reaction 16 can be described as:

$$\frac{d[-\text{NH}_2]}{dt} = -\frac{d[\text{NH}_3(\text{ad})]}{dt} = k_3[\text{NH}_3(\text{ad})][\text{Mn}^{4+}] \quad (20)$$

where k_3 and $[-\text{NH}_2]$ are the kinetic constant of reaction 16 and the concentration of -NH₂ on MnO_x/TiO₂, respectively.

The kinetic equation of reaction 17 can be described as:

$$\frac{d[-\text{NH}]}{dt} = -\frac{d[-\text{NH}_2]}{dt} = k_4[-\text{NH}_2][\text{Mn}^{4+}] \quad (21)$$

where k_4 and $[-\text{NH}]$ are the kinetic constant of reaction 17 and the concentration of -NH on MnO_x/TiO₂.

The kinetic equations of reactions 18 and 19 can be described as:

$$\frac{d[\text{N}_2]}{dt} = -\frac{d[-\text{NH}_2]}{dt} = -\frac{d[\text{NO}(\text{g})]}{dt} = k_5[-\text{NH}_2][\text{NO}(\text{g})] \quad (22)$$

$$\frac{d[\text{N}_2\text{O}]}{dt} = -\frac{d[-\text{NH}]}{dt} = -\frac{d[\text{NO}(\text{g})]}{dt} = k_6[-\text{NH}][\text{NO}(\text{g})] \quad (23)$$

where, k_5 , k_6 and $[\text{NO}(\text{g})]$ are the kinetic constants of reactions 18 and 19, and the concentration of gaseous NO, respectively.

According to eqn (20)–(22), the variation of -NH₂ concentration on MnO_x/TiO₂ can be described as:

$$-\frac{d[-\text{NH}_2]}{dt} = k_5[-\text{NH}_2][\text{NO}(\text{g})] + k_4[-\text{NH}_2][\text{Mn}^{4+}] - k_3[\text{NH}_3(\text{ad})][\text{Mn}^{4+}] \quad (24)$$

As the reaction reached the steady state, -NH₂ concentration on MnO_x/TiO₂ would not vary. Therefore,

$$-\frac{d[-\text{NH}_2]}{dt} = 0 \quad (25)$$

Thus,

$$[-\text{NH}_2] = \frac{k_3[\text{NH}_3(\text{ad})][\text{Mn}^{4+}]}{k_5[\text{NO}(\text{g})] + k_4[\text{Mn}^{4+}]} \quad (26)$$

Then, the formation of N₂ (eqn (22)) can be transformed as:

$$\frac{d[\text{N}_2]}{dt} = k_5[\text{NO}(\text{g})] \frac{k_3[\text{NH}_3(\text{ad})][\text{Mn}^{4+}]}{k_5[\text{NO}(\text{g})] + k_4[\text{Mn}^{4+}]} = k_5 \frac{k_3[\text{NH}_3(\text{ad})][\text{Mn}^{4+}]}{k_5 + k_4 \frac{[\text{Mn}^{4+}]}{[\text{NO}(\text{g})]}} \quad (27)$$

According to eqn (21) and (23), the variation of -NH concentration on MnO_x/TiO₂ can be described as:

$$\frac{d[-\text{NH}]}{dt} = k_4[-\text{NH}_2][\text{Mn}^{4+}] - k_6[-\text{NH}][\text{NO}(\text{g})] \quad (28)$$

As the reaction reached the steady state, -NH concentration on MnO_x/TiO₂ would not vary. Therefore,

$$\frac{d[-\text{NH}]}{dt} = 0 \quad (29)$$

Thus,

$$[-\text{NH}] = \frac{k_4[-\text{NH}_2][\text{Mn}^{4+}]}{k_6[\text{NO}(\text{g})]} = \frac{k_3[\text{NH}_3(\text{ad})][\text{Mn}^{4+}]}{k_5[\text{NO}(\text{g})] + k_4[\text{Mn}^{4+}]} \cdot \frac{k_4[\text{Mn}^{4+}]}{k_6[\text{NO}(\text{g})]} \quad (30)$$

Then, the formation of N₂O (eqn (23)) can be transformed as:

$$\begin{aligned} \frac{d[\text{N}_2\text{O}]}{dt} &= k_6[\text{NO}(\text{g})] \frac{k_3[\text{NH}_3(\text{ad})][\text{Mn}^{4+}]}{k_5[\text{NO}(\text{g})] + k_4[\text{Mn}^{4+}]} \cdot \frac{k_4[\text{Mn}^{4+}]}{k_6[\text{NO}(\text{g})]} \\ &= \frac{k_3[\text{NH}_3(\text{ad})][\text{Mn}^{4+}]}{k_5[\text{NO}(\text{g})] + k_4[\text{Mn}^{4+}]} (k_4[\text{Mn}^{4+}]) \end{aligned} \quad (31)$$

Taking account of the contributions of both the Langmuir–Hinshelwood mechanism and the Eley–Rideal mechanism,

the formation of N_2 and N_2O can be approximately described as follows:

$$\frac{d[N_2]}{dt} = k_1[NH_4NO_2] + k_5 \frac{k_3[NH_{3(ad)}][Mn^{4+}]}{k_5 + k_4 \frac{[Mn^{4+}]}{[NO_{(g)}]}} \quad (32)$$

$$\frac{d[N_2O]}{dt} = k_2[NH_4NO_3] + \frac{k_3[NH_{3(ad)}][Mn^{4+}]}{k_5[NO_{(g)}] + k_4[Mn^{4+}]} (k_4[Mn^{4+}]) \quad (33)$$

The concentrations of NH_4NO_2 and NH_4NO_3 on MnO_x/TiO_2 were independent of gaseous NO and NH_3 , so the contribution of the Langmuir–Hinshelwood mechanism to the formation of N_2 and N_2O would not vary after the increase of gaseous NO concentration. However, the contribution of the Eley–Rideal mechanism to N_2 formation would increase after the increase of gaseous NO concentration (hinted by eqn (32)). Meanwhile, the contribution of the Eley–Rideal mechanism to N_2O formation would decrease after the increase of gaseous NO concentration (hinted by eqn (33)).

If the reduction of NO mainly followed the Langmuir–Hinshelwood mechanism, N_2O selectivity can be described as:

$$N_2O \text{ selectivity} = \frac{C_{N_2O}}{C_{N_2O} + C_{N_2}} = \frac{k_2[NH_4NO_3]}{k_1[NH_4NO_2] + k_2[NH_4NO_3]} \quad (34)$$

The concentrations of NH_4NO_2 and NH_4NO_3 did not change after the increase of gaseous NO and NH_3 , so N_2O selectivity was independent of gaseous NO concentration.

If the reduction of NO mainly followed the Eley–Rideal mechanism, N_2O selectivity can be described as:

$$N_2O \text{ selectivity} = \frac{C_{N_2O}}{C_{N_2O} + C_{N_2}} = \frac{k_4[Mn^{4+}]}{k_5[NO_{(g)}] + k_4[Mn^{4+}]} \quad (35)$$

Eqn (35) suggests that N_2O selectivity would decrease after the increase of gaseous NO concentration.

There is generally agreement that the Langmuir–Hinshelwood mechanism plays an important role on the SCR reaction at lower temperatures.^{3,6} Meanwhile, the Eley–Rideal mechanism can also contribute to NO reduction at lower temperatures. The Eley–Rideal mechanism was obviously promoted with the increase of reaction temperature and it predominated over the SCR reaction at higher temperatures.^{3,6}

4.2 Effect of gaseous NO concentration in the inlet on N_2O selectivity

If the concentrations of gaseous NO and NH_3 were sufficiently high, the whole catalyst bed was saturated with the adsorption of gaseous NO and NH_3 . Thus, $[NH_{3(ad)}]$, $[NH_4NO_2]$ and $[NH_4NO_3]$ can be regarded as constants on the whole catalyst bed. However, the concentration of gaseous NO at the bottom of the catalyst bed was much less than that at the top of the catalyst bed due to the reduction of NO. Therefore, the

amounts of N_2 and N_2O formed over the whole catalyst bed should be described as follows:

$$C_{N_2} = k_1[NH_4NO_2]t + \int_0^t k_5 \frac{k_3[NH_{3(ad)}][Mn^{4+}]}{k_5 + k_4 \frac{[Mn^{4+}]}{[NO_{(g)}]_t}} dt \quad (36)$$

$$C_{N_2O} = k_2[NH_4NO_3]t + \int_0^t \frac{k_3[NH_{3(ad)}][Mn^{4+}]}{k_5[NO_{(g)}]_t + k_4[Mn^{4+}]} (k_4[Mn^{4+}]) dt \quad (37)$$

where t is the time how long gaseous NO passed through the catalyst column, which is inversely proportional to the GHSV.

Fig. 7a shows that the concentrations of gaseous NO in the outlet of the reaction with 1000 ppm of NO and 500 ppm of NH_3 were much higher than that with 500 ppm of NO and 500 ppm of NH_3 . Meanwhile, the concentration of gaseous NO in the inlet of the reaction with 1000 ppm of NO and 500 ppm of NH_3 were twice that with 500 ppm of NO and 500 ppm of NH_3 . They suggest that the concentrations of gaseous NO at each section of the catalyst bed during the reaction with 1000 ppm of NO and 500 ppm of NH_3 were all higher than those with 500 ppm of NO and 500 ppm of NH_3 . Hinted by eqn (36), the amount of N_2 formed during the reaction with 1000 ppm of NO and 500 ppm of NH_3 was higher than that with 500 ppm of NO and 500 ppm of NH_3 , which was demonstrated in Fig. 7c. Hinted by eqn (37), the amount of N_2O formed during the reaction with 1000 ppm of NO and 500 ppm of NH_3 was less than that with 500 ppm of NO and 500 ppm of NH_3 , which was demonstrated in Fig. 7d. As a result, N_2O selectivity of the reaction with 1000 ppm of NO and 500 ppm of NH_3 was less than that with 500 ppm of NO and 500 ppm of NH_3 (shown in Fig. 2b).

The concentrations of gaseous NO in the outlet and in the inlet during the reaction with 1000 ppm of NO and 1000 ppm of NH_3 were both close to those with 1000 ppm of NO and 500 ppm of NH_3 below 200 °C (shown in Fig. 7a). It suggests that the concentrations of gaseous NO at each section of the catalyst bed during the reaction with 1000 ppm of NO and 1000 ppm of NH_3 were all close to those with 1000 ppm of NO and 500 ppm of NH_3 below 200 °C. Therefore, the amounts of N_2 and N_2O formed during the reaction with 1000 ppm of NO and 1000 ppm of NH_3 were close to those with 1000 ppm of NO and 500 ppm of NH_3 below 200 °C, which is demonstrated in Fig. 7c and d. As a result, N_2O selectivity of the reaction with 1000 ppm of NO and 1000 ppm of NH_3 was close to that with 1000 ppm of NO and 500 ppm of NH_3 below 200 °C (shown in Fig. 2b). However, little NH_3 can be observed in the outlet of the reaction with 1000 ppm of NO and 500 ppm of NH_3 above 200 °C (shown in Fig. 7b). It suggests that some catalyst in the bottom of the catalyst bed did not take part in the reaction because gaseous NH_3 had been completely consumed. As the concentration of gaseous NH_3 increased from 500 to 1000 ppm, a large amount of NH_3 can be observed in the outlet above 200 °C (shown in Fig. 7b). Therefore, most of

the catalyst took part in the reaction with 1000 ppm of NO and 1000 ppm of NH₃ above 200 °C. They suggest that *t* of the reaction with 1000 ppm of NO and 1000 ppm of NH₃ was higher than that with 1000 ppm of NO and 500 ppm of NH₃ above 200 °C. Hinted by eqn (36) and (37), the amounts of N₂ and N₂O formed during the reaction with 1000 ppm of NO and 1000 ppm of NH₃ above 200 °C were both much higher than that with 1000 ppm of NO and 500 ppm of NH₃ (shown in Fig. 7c and d). Gaseous NO concentration at the top of the catalyst bed was much higher than that at the bottom of the catalyst bed due to NO reduction. It suggests that N₂O selectivity at the top of the catalyst bed was much less than that at the bottom of the catalyst bed. As a result, N₂O selectivity of the reaction with 1000 ppm of NO and 1000 ppm of NH₃ above 200 °C were higher than that with 1000 ppm of NO and 500 ppm of NH₃, which was demonstrated in Fig. 2b.

Fig. 7a shows that the concentrations of gaseous NO at each section of the catalyst column during the reaction with 1000 ppm of NO and 1000 ppm of NH₃ were all higher than those with 500 ppm of NO and 500 ppm of NH₃. Hinted by eqn (35), N₂O selectivity of the reaction with 1000 ppm of NO and 1000 ppm of NH₃ was less than that with 500 ppm of NO and 500 ppm of NH₃ (shown in Fig. 2b).

5. Conclusion

N₂O selectivity of the low temperature SCR reaction over MnO_x/TiO₂ was related to gaseous NO concentration in the flue gas. The lower concentration of gaseous NO in the flue gas would cause the higher N₂O selectivity. If the concentration of gaseous NO in the flue gas is very low, low temperature SCR of NO with MnO_x/TiO₂ as the catalyst could not be the right choice for the control of NO emission due to the lower N₂ selectivity. Furthermore, N₂O selectivity at the bottom of the catalyst bed was much higher than that at the top of the catalyst column due to the lower gaseous NO concentration. Therefore, the decrease of GHSV to excessively pursue the removal efficiency of NO will cause lower N₂ selectivity.

Acknowledgements

This study was financially supported by the National Natural Science Fund of China (Grant No. 21207067 and 41372044), Environmental scientific research of Jiangsu Province (2012026), the Fundamental Research Funds for the Central Universities (grant no. 30920130111023), the Zijin Intelligent Program, Nanjing University of Science and Technology (grant no. 2013-0106), and special fund of State Key Joint Laboratory of Environment Simulation and Pollution Control.

Notes and references

- G. S. Qi and R. T. Yang, *J. Catal.*, 2003, **217**, 434–441.
- N. Y. Topsoe, *Science*, 1994, **265**, 1217–1219.
- G. Busca, L. Lietti, G. Ramis and F. Berti, *Appl. Catal., B*, 1998, **18**, 1–36.
- S. J. Yang, J. H. Li, C. Z. Wang, J. H. Chen, L. Ma, H. Z. Chang, L. Chen, Y. Peng and N. Q. Yan, *Appl. Catal., B*, 2012, **117**, 73–80.
- Y. Liu, T. T. Gu, X. L. Weng, Y. Wang, Z. B. Wu and H. Q. Wang, *J. Phys. Chem. C*, 2012, **116**, 16582–16592.
- S. J. Yang, C. Z. Wang, J. H. Li, N. Q. Yan, L. Ma and H. Z. Chang, *Appl. Catal., B*, 2011, **110**, 71–80.
- G. S. Qi, R. T. Yang and R. Chang, *Appl. Catal., B*, 2004, **51**, 93–106.
- G. S. Qi and R. T. Yang, *J. Phys. Chem. B*, 2004, **108**, 15738–15747.
- P. G. Smirniotis, P. M. Sreekanth, D. A. Pena and R. G. Jenkins, *Ind. Eng. Chem. Res.*, 2006, **45**, 6436–6443.
- Z. B. Wu, B. Q. Jiang, Y. Liu, H. Q. Wang and R. B. Jin, *Environ. Sci. Technol.*, 2007, **41**, 5812–5817.
- B. Q. Jiang, Y. Liu and Z. B. Wu, *J. Hazard. Mater.*, 2009, **162**, 1249–1254.
- Y. J. Kim, H. J. Kwon, I. S. Nam, J. W. Choung, J. K. Kil, H. J. Kim, M. S. Cha and G. K. Yeo, *Catal. Today*, 2011, **151**, 244–250.
- S. M. Lee, K. H. Park, S. S. Kim, D. Kwon and S. C. Hong, *J. Air Waste Manage. Assoc.*, 2012, **62**, 1085–1092.
- Z. B. Wu, R. B. Jin, Y. Liu and H. Q. Wang, *Catal. Commun.*, 2008, **9**, 2217–2220.
- G. S. Qi and R. T. Yang, *Appl. Catal., B*, 2003, **44**, 217–225.
- P. G. Smirniotis, D. A. Pena and B. S. Uphade, *Angew. Chem., Int. Ed.*, 2001, **40**, 2479–2481.
- M. Wallin, S. Forser, P. Thormahlen and M. Skoglundh, *Ind. Eng. Chem. Res.*, 2004, **43**, 7723–7731.
- D. A. Pena, B. S. Uphade and P. G. Smirniotis, *J. Catal.*, 2004, **221**, 421–431.
- D. A. Pena, B. S. Uphade, E. P. Reddy and P. G. Smirniotis, *J. Phys. Chem. B*, 2004, **108**, 9927–9936.
- S. Roy, B. Viswanath, M. S. Hegde and G. Madras, *J. Phys. Chem. C*, 2008, **112**, 6002–6012.
- X. F. Tang, J. H. Li, L. A. Sun and J. M. Hao, *Appl. Catal., B*, 2010, **99**, 156–162.
- G. Madia, M. Koebel, M. Elsener and A. Wokaun, *Ind. Eng. Chem. Res.*, 2002, **41**, 4008–4015.
- G. Delahay, B. Coq, S. Kieger and B. Neveu, *Catal. Today*, 1999, **54**, 431–438.
- M. H. Kim and S. W. Ham, *Top. Catal.*, 2010, **53**, 597–607.
- S. Suarez, J. A. Martin, M. Yates, R. Avila and J. Blanco, *J. Catal.*, 2005, **229**, 227–236.
- L. A. Chen, J. H. Li and M. F. Ge, *Environ. Sci. Technol.*, 2010, **44**, 9590–9596.
- P. R. Ettireddy, N. Ettireddy, S. Mamedov, P. Boolchand and P. G. Smirniotis, *Appl. Catal., B*, 2007, **76**, 123–134.
- K. Zhuang, J. Qiu, F. S. Tang, B. L. Xu and Y. N. Fan, *Phys. Chem. Chem. Phys.*, 2011, **13**, 4463–4469.
- F. D. Liu, K. Asakura, H. He, W. P. Shan, X. Y. Shi and C. B. Zhang, *Appl. Catal., B*, 2011, **103**, 369–377.
- K. I. Hadjiivanov, *Catal. Rev.*, 2000, **42**, 71–144.